Scientia Iranica B (2014) 21(5), 1621–1634

SCIENTIA IRANICA

Sharif University of Technology
Scientia Iranica
Transactions B: Mechanical Engineering
www.scientiairanica.com

CFD based optimization of the mixture formation in spark ignition direct injection CNG engine

I. Chitsaz[a,b], M.H. Saidi[a,*] and A.A. Mozafari[a]

a. *Center of Excellence in Energy Conversion (CEEC), School of Mechanical Engineering, Sharif University of Technology, Tehran, P.O. Box 11155-9567, Iran.*
b. *Department of Laboratory, Iran Khodro Power Train Co. (IP-CO), Tehran, P.O. Box 1398813711, Iran.*

Received 12 April 2012; received in revised form 6 November 2013; accepted 25 January 2014

KEYWORDS
CNG-DI;
Mixture formation;
Optimization;
Genetic algorithm;
Bowl geometry.

Abstract. This paper describes optimization of the combustion chamber geometry and injection timing of a new generation of EF7 engine, where CNG is directly injected to the combustion chamber, with the aim of providing the best mixture at low and high speeds. The Multi-Objective Genetic Algorithm (MOGA) is coupled with the KIVA Computational Fluid Dynamics (CFD) code, with grid generation, in order to maximize the flammable mass of the mixture. This would result in better combustion and improved fuel economy. The optimization variables related to the combustion chamber are seven geometry variables and injection timing. Through the present optimization, a great improvement in mixture distribution is achieved. The optimization results show that early injection with a shallow bowl shape can be advantageous at high speeds, while late injection would result in better results at low speeds.

© 2014 Sharif University of Technology. All rights reserved.

1. Introduction

Compressed Natural Gas-Direct Injection (CNG-DI) engine development has now become a challenging and innovative technology. Due to the growing importance of future emission restrictions, manufacturers of internal combustion engines are forced continuously to optimize combustion chamber design for improvement of the mixture formation and combustion process [1]. Direct injection in internal combustion engines enables realization of stratified charges and seems to be the most promising way [2-4] of improving fuel economy in spark-ignition engines. Mixture distribution of stratified direct injection is very important for more stable combustion and lower emissions.

High capacity computers have enabled wider application of computational fluid dynamics modeling in engine design. Mixture distribution affects combustion efficiency, engine output and emissions. Thus, in order to maximize fuel economy, optimization of the fuel-air mixture formation is essential for different engine operating conditions or various combustion bowl shapes. This motivates engine designers to combine optimization processes with numerical work.

Some previous studies were conducted on natural gas direct-injection combustion using a rapid compression machine or engine [5-11]. Zeng et al. [5,6] investigated the combustion characteristics of a direct injection natural gas engine under various fuel injection timings. The effect of fuel injection timing relative to ignition timing for natural gas direct-injection in a rapid compression machine [6,7,9,10] were studied, and the characteristics of combustion and emissions of CNG-DI combustion [8] were evaluated. It was shown that the compression ratio should be higher than 10, and a compression ratio of 12 provided the best results for the engine, employed by Zheng et al. [11]. Hassan et al. [12] and Kalam and Masjuli [13] presented

*. *Corresponding author. Tel.: +98 21 66165522; Fax: +98 21 66000021*
E-mail address: Saman@sharif.edu (M.H. Saidi)

a converted CNG-DI engine that has some benefits in BSFC, NOx, while a great penalty is observed for HC and CO emissions. This penalty is due to the same compression ratio for CNG-DI, CNG-BI and gasoline-PI. Sen et al. [14] investigated the time series of the indicated mean effective pressure of CNG-DI using wavelet to find the dominant oscillatory modes. Tadesse and Aziz [15] presented the effect of boost pressure on engine performance and exhaust emissions. An experimental study was conducted on a 4-stroke direct injection compressed natural gas spark ignition engine with compression ratio of 14. They concluded that partial direct injection gives better performance for speeds of 2000 compared to early injection timings. They also found that early injection timing with boost pressure gives better performance for engine speeds of 4000 to 5000 RPM, compared to partial direct injection, due to sufficient available time for mixture preparation.

Abdullah et al. [16] performed a numerical simulation on a single cylinder 1.6 liter engine running at wide open throttle. They concluded that fuel injection timing plays an important role in engine performance, combustion and emissions, because it influences the time of fuel air mixing shortly before spark ignition begins. The retardation of fuel injection reduces CO in the exhaust but increases NO emission, due to excess air in the mixture, and decreases combustion pressure. Agarwal and Assanis [17] undertook a numerical work to investigate heat release and pollutant formation processes in a CNG-DI engine. They showed that the use of detailed chemistry was extremely important for predicting the correct ignition delay period under different engine operating conditions. Baratta et al. [18] applied a Star-CD based model for investigation of the direct natural gas injection process from a poppet-valve injector into a bowl-piston engine combustion chamber. The numerical procedure was validated through comparison of numerical results with Schlieren images of the jet profile in a constant-volume bomb. Several studies have been focused on CFD based optimization in engine design. Mohd Ali et al. [19] presented the gas-jet ignition method to extend the lean combustible limit of CNG engines. Their results showed that a CNG engine can be operated at equivalence ratio ranges from 0.3 and 0.8 by applying a two-stage injection combined with gas-jet ignition. Their experimental and numerical efforts showed that combustion stability and emissions are affected by fuel distribution. Andreassi et al. [20] applied a single cylinder direct injection for the direct injection of a small quantity of natural gas through the spark plug. They also performed numerical work to improve the micro-direct injection PSC process. Andreassi et al. [21] also presented an analysis of different injection strategies to demonstrate that these tools are suitable for optimization of direct injection gas engines. In their numerical effort, the main performance parameters, such as maximum pressure, maximum temperature, heat rate curve and burned fuel mass fraction, have been considered to achieve a better comprehension of the physical phenomena involved in the engine. Douailler et al. [22] performed a 3D CFD simulation and an experimental test on the converted diesel engine. They modified and designed a new cylinder head and piston crown to optimize combustion velocity after their simulations. Mohamad et al. [23] used a spark plug fuel injector for the conversion of port fuel injection to direct injection of natural gas. They showed that there is pressure loss in the fuel injection of natural gas but a spark plug gaseous injector improves volumetric efficiency. Research into the effects of different injection strategies, injector types and piston crown geometries on the mixture formation of a direct injected turbocharged CNG-engine was carried out by Chiodi et al. [24]. They followed homogeneous and stratified mixture formation to realize the effects of mixture formation on combustion.

Kurniawan et al. [25,26] applied a neural network as an artificial intelligence tool to determine the performance and emissions in a compressed natural gas direct injection engine. They used 15 data acquired from CFD combustion simulation to characterize the combustion behavior of such engines used for the training process of artificial neural networks. They concluded that the best strategy for achieving higher power, lower CO, and NO emissions was to advance the start of injection timing and delay the end of injection timing with earlier spark advanced timing. They [27] also optimized the combustion process of compressed natural gas direct injection using the coupled CFD and multi-objective genetic algorithm code, in order to improve engine performance and emissions. Their objectives were optimized by a variation in start of injection, end of injection and spark ignition timing at a speed of 2000 rpm. Engine power output and exhaust emissions were also considered important parameters as objective functions.

For development of the CNG-DI engine operated under different loads, the mixture formation varies considerably, which results in different injection timing and combustion chamber shapes. It can be anticipated that different injection strategies and matching of piston geometry are needed for engines under different operating conditions in order to get better results. In previous work, the optimized geometry and operating condition of CNG-DI has not yet been studied, and all optimization research is confined to engine output, while mixture distribution has a critical role. In the present study, a CFD based optimization is used to simulate mixture formation of a CNG-DI engine in EF7 and to study the effects of bowl geometry and injection

timing on the engine. The optimized combinations of piston bowl geometry and injection timing are considered to improve fuel economy at low and high speeds. This investigation into the CNG-DI engine has not been undertaken in existing literature. Moreover, the optimization process applied here allows several objectives to be contemporarily optimized; the effects of injection timing and combustion bowl geometry are also considered.

2. Mathematical model

In the present study, simulations were performed using the KIVA3V [28] code, which was coupled with a genetic algorithm and mesh generation with KIVA-Prep in order to optimize the combustion bowl geometry and injection timing. The volume of the piston bowl was kept constant for all cases to keep the compression ratio unchanged. A second order upwind scheme was used to discretize both momentum and continuity equations. The closed-loop of the engine cycle was simulated and the turbulent flow was modeled by a modified renormalization group (RNG) k-ε model [29]. Natural Gas injection in KIVA is modeled by the Ra et al. [30] procedure. In this method, the inflow conditions were calculated using the under-expanded jet model and the similarity solution [31]. The effective nozzle diameter for the similarity solution was assigned to the size of the Mach disk, and the velocity at the effective nozzle exit was assumed to be sonic. The mass flow rate of the jet was calculated at the distance where the jet's half-velocity width was equal to the size of the inflow boundary cell of the computational grid.

2.1. Engine description and operating conditions

A single-cylinder, direct injection, four-stroke SI engine, based on an EF7, was used in the modeling. The main geometric specifications and fuel injector parameters are summarized in Table 1. Due to the limited space for mounting the injector in the EF7 cylinder head, a spark plug fuel injector is selected for the injection system. This means that the injector is one hole, centrally mounted in the cylinder head. The base piston bowl geometry is determined, based on Baratta et al. [18]. However, slight changes were made in the present modeling work, such as axisymmetric simulations. Bowl geometry was modified and also the stroke was increased from 82.5 to 95 to increase the compression ratio. The piston geometry and cylinder head are shown in Figure 1, where z is axisymmetric of the geometry.

Table 1. Engine and injector specification.

Baseline engine	EF7 SI engine
Bore × stroke (mm)	78.6 × 95
Fisplacement (liter)	2.0
Connecting rod length (mm)	134.5
Guel injector nozzles	Axisymmetric nozzle
Tail pressure (bar)	30
Nozzle orifice diameter (mm)	0.225 mm
Compression ratio	12.24
Equivalence ratio	Stoichiometric
Swirl ratio	2.8

2.2. Grid-size independency

To avoid grid-size dependency, four mesh sizes with the same conditions were used to check the mesh dependency of the problem. The methane mass fractions of the axisymmetric line (AH in Figure 1) for different mesh sizes are given in Figure 2. As shown, the methane mass fraction along the axis approximately

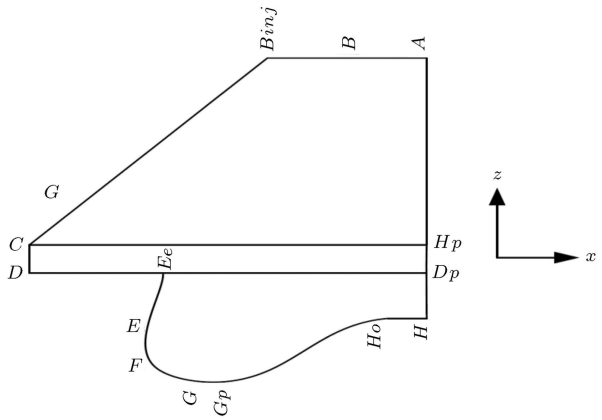

Figure 1. Computational grid based on EF7 engine and Baratta et al. simulations [18].

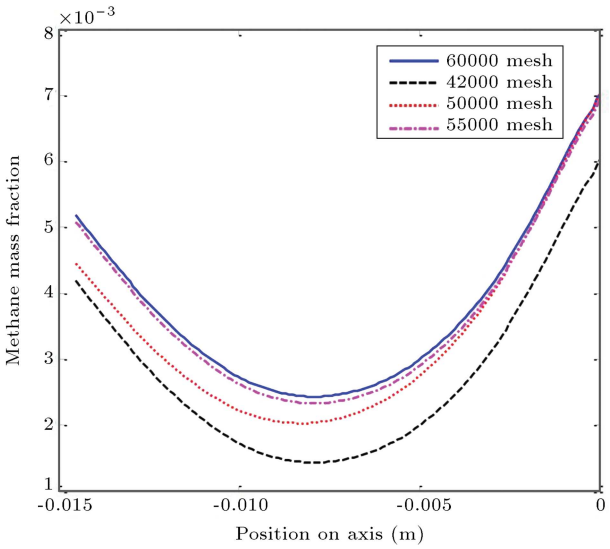

Figure 2. Methane mass fraction of four mesh size at TDC.

Table 2. Design variables and objectives.

Design variables	Range	
	800 rpm	**2000 rpm**
z_{G_p} (mm)	-30 to -26	-30 to -26
z_G (mm)	-30 to -26	-30 to -26
z_F (mm)	-25.5 to -21.5	-25.5 to -21.5
z_E (mm)	-22.9 to -18.9	-22.9 to -18.9
x_{E_e} (mm)	-22 to -20	-22 to -20
x_E (mm)	-20.8 to -19.5	-20.8 to -19.5
x_G (mm)	-18.7 to -17.7	-18.7 to -17.7
x_{G_p} (mm)	-18 to -16.7	-18 to -16.7
Injection timing	180 BTDC to 20 BTDC	180 BTDC to 20 BTDC
Objectives:		
Flammable mixture in the vicinity of spark plug		
Flammable mixture in the cylinder		

does not change after refinement of 55000 meshes. As a compromise between computational efficiency and model accuracy requirements, the cell size was specified as 0.2 mm in this work.

2.3. Optimization parameters and objectives

In order to analyze a wide range of piston crown shapes, a parametric grid generator is developed. In this grid generation, five parametric points of H, G, F, E and Ee, in Figure 1, are varied to construct new piston crown shapes to keep the compression ratio constant. In addition, the start of injection which is one of operating conditions, is optimized.

There are a number of methods applied to quantify the mixing performance of a given gas injector [32,33]. The mixture that fills each computational finite volume can belong to three categories: too lean, flammable and too rich. Too lean and rich mixtures cause the flame to quench or can be led to misfire at the start of combustion. Therefore, a flammable mixture would result in stable combustion. It is also notable that unburned hydrocarbon and NOx emission would be increased, due to the too rich and too lean mixtures in the engine operating condition, respectively. Therefore, flammable mass distribution increases the performance of the engine and also reduces the engine emissions. In other words, the flammable mass fraction of the fuel is related to combustion efficiency, as it indicates the relative mass of fuel that is combustible [33].

The objectives of engine optimization include both the flammable mass fraction of the mixture at the time of ignition in the cylinder, and the flammable mixture in the vicinity of the spark plug. The flammable mass fraction of the mixture is defined as the ratio of the flammable mass of the mixture to the total mass of the mixture in the cylinder, which is written as:

$$f_m = \frac{\text{Flammable mass of mixture}}{\text{Total mass of mixture}}. \quad (1)$$

Optimization parameters and objectives are summarized in Table 2.

2.4. Micro genetic algorithm

In the present study, the optimization process is performed with the multi objective micro genetic algorithm that was already tested for engine application by Park [34]. This optimization process is used to optimize combustion bowl geometry as well as injection timing in the CNG-DI engine. The multi-objective optimization approach, based on a micro genetic algorithm (micro-GA), a genetic algorithm with a very small population (five individuals), was used in our experiment. The algorithm starts from a random initial population of binary strings and calculates the fitness of each individual ranked according to Pareto optimally criterion. The Pareto optimal solutions consist of solutions that are not dominated by any other solutions, where the concept of domination is defined as:

$$m < n \Leftrightarrow \forall i(m_i \leq n_i) \wedge \exists i(m_i < n_i). \quad (2)$$

For an optimization where the minimization of each objective is sought (such as minimizing emissions and fuel consumption), when Eq. (2) is met, m is said to be dominated by n [35]. Figure 3 [36] shows that designs A to D are Pareto optimal solutions. The best individuals, those that have strings with high

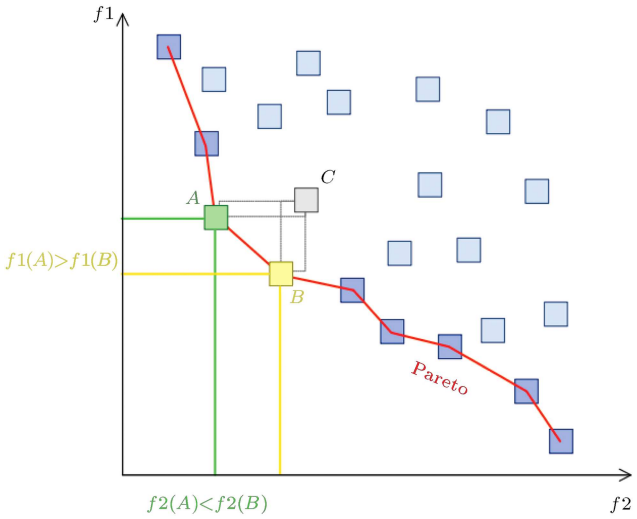

Figure 3. Pareto optimal solutions [36].

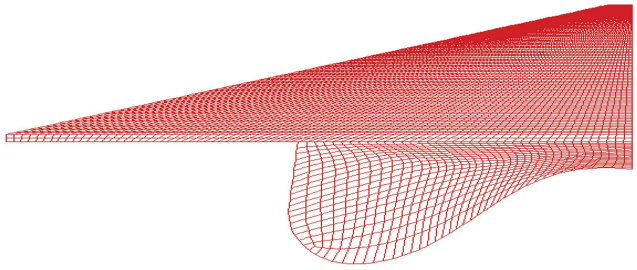

Figure 4. Computational mesh of the baseline engine at the top dead center.

overall fitness values, are selected for reproduction, while their chromosomes are exchanged with the single point crossover technique. In this optimization, elitism is also applied, by replacing some strings from the new population with individuals from the Pareto optimal solution. The new generation is used as starting generation until convergence is met. In order to perform the optimization process, the baseline bowl geometry needs to be generated based on variables related to the chamber geometry. Therefore, the piston bowl geometry of the baseline engine was modeled as the mesh shown in Figure 4.

2.5. Injection model

Due to the focus of this research being on mixture formation, numerical gaseous injection should also be validated. Gaseous injection is the start of mixture formation, and the accuracy of numerical simulation has a great effect on the results. In the present study, it is assumed that the fluid is compressible and Newtonian with temperature-dependent fluid properties. A numerical solution of the mean flow and thermal fields requires resolving the continuity equations: Reynolds averaged Navier-Stokes equation, time-averaged energy equation, species transport equation and ideal gas relation [37]:

$$\frac{\partial(\rho\bar{u}_i)}{\partial x_i} = 0, \tag{3}$$

$$\left(\frac{\partial(\rho\bar{u}_i\bar{u}_j)}{\partial x_j}\right) = -\frac{\partial P}{\partial x_i} + \frac{\partial}{\partial x_j}\left[\mu\left(\frac{\partial\bar{u}_i}{\partial x_j} + \frac{\partial\bar{u}_j}{\partial x_i} - \frac{2}{3}\delta_{ij}\frac{\partial\bar{u}_l}{\partial x_l}\right)\right] - \frac{\partial}{\partial x_j}\left(\rho\overline{u_i'u_j'}\right), \tag{4}$$

$$\frac{\partial}{\partial x_i}\left[\bar{u}_i\left(\rho\overline{Y_j h}_j + \rho\frac{\bar{u}^2}{2}\right)\right] = \frac{\partial}{\partial x_i}\left(K\frac{\partial\bar{T}}{\partial x_i} - \rho\overline{u_i'T'}\right) + \frac{\partial}{\partial x_i}\left[\overline{h_j}\left(\rho D_{j,k} + \frac{\mu_t}{Sc_t}\right)\frac{\partial Y_j}{\partial x_i}\right], \tag{5}$$

$$\frac{\partial(\rho\bar{u}_j Y_i)}{\partial x_j} = \frac{\partial}{\partial x_j}\left[\left(\rho D_{i,k} + \frac{\mu_t}{Sc_t}\right)\frac{\partial Y_i}{\partial x_j}\right], \tag{6}$$

$$P = \rho RT. \tag{7}$$

Enthalpy in Eq. (5) is defined by Eq. (8):

$$\bar{h}_j = \int_{298.15}^{T} C_{p,j}dT. \tag{8}$$

As shown in Eqs. (4) and (5), additional terms, $-\rho\overline{u_i'u_j'}$ and $\rho\overline{u_i'T'}$, were entered in the energy and Navier-Stokes equations. Additional terms should be modeled. Boussinesq represent a fundamental equation that is shown in Eq. (9). Some turbulence models, such as k-ε, use this fundamental equation:

$$\rho\overline{u_i'u_j'} = -\mu_t\left(\frac{\partial\bar{u}_i}{\partial x_j} + \frac{\partial\bar{u}_j}{\partial x_i}\right) + \frac{2}{3}\left(\rho k + \mu_t\frac{\partial\bar{u}_l}{\partial x_l}\right)\delta_{ij},$$

$$\overline{u_i'T'} = -\frac{C_p\mu_t}{\rho\,\mathrm{Pr}_t}\left(\frac{\partial\overline{T}}{\partial x_i}\right). \tag{9}$$

In Boussinesq approximation, Reynolds stress is related to the local velocity gradients introducing the eddy viscosity, v_t. The turbulence quantities (k and ε) used to calculate v_t are determined from the following modeled transport equations. The presented turbulent flow was modeled by a modified renormalization group (RNG) k-ε model [29]:

$$\rho\frac{\partial k}{\partial t} = \frac{\partial}{\partial x_i}\left(\alpha_k\mu_{eff}\frac{\partial k}{\partial x_i}\right) + \mu_t\frac{\sqrt{2}}{2}\left(\frac{\partial\bar{u}_i}{\partial x_j} + \frac{\partial\bar{u}_j}{\partial x_i}\right) - \rho\varepsilon - 2\rho\varepsilon\frac{k}{\gamma RT}, \tag{10}$$

$$\rho\frac{\partial\varepsilon}{\partial t} = \frac{\partial}{\partial x_i}\left(\alpha_\varepsilon\mu_{eff}\frac{\partial\varepsilon}{\partial x_i}\right) + 1.42\frac{\varepsilon}{k}\mu_t \times\frac{\sqrt{2}}{2}\left(\frac{\partial\bar{u}_i}{\partial x_j} + \frac{\partial\bar{u}_j}{\partial x_i}\right) - 1.68\rho\frac{\varepsilon^2}{k} - R, \tag{11}$$

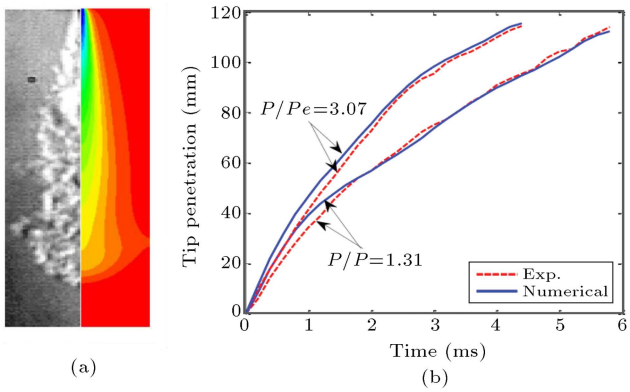

Figure 5. Numerical and experimental data of gaseous injection: (a) Helium density of simulated and experimental results in pressure ratio 1.31 and $d = 1$ mm at 4 ms; and (b) tip penetration comparisons of experimental and numerical data at $d = 1$ mm.

$$\mu_t = C_\mu \frac{\rho k^2}{\varepsilon}, \tag{12}$$

where C_μ, α_k and α_ε are constants that equal 0.0845, 1.393 and 1.393, respectively.

The main difference between the RNG and standard k-ε models lies in the additional term in the ε equation, given by:

$$R = \frac{C_\mu \rho \eta^3 (1 - \eta/\eta_0)}{1 + \beta \eta^3} \frac{\varepsilon^2}{k}, \tag{13}$$

where:

$$\eta \equiv k/\varepsilon \times \mu_t \times \frac{\sqrt{2}}{2} \left(\frac{\partial \bar{u}_i}{\partial x_j} + \frac{\partial \bar{u}_j}{\partial x_i} \right),$$

$$\eta_0 = 4.38, \qquad \beta = 0.012.$$

In regions where $\eta < \eta_0$, the R term makes a positive contribution. As a result, for weakly to moderately strained flow, the RNG model tends to give more turbulence in comparison to the standard k-ε model.

To evaluate model accuracy, tip penetration of the helium injection is validated and shown in Figure 5. The density contours of the present computations are also compared to the experimental ones extracted from the Schlieren [38]. As shown in this figure, tip penetration is predicted quite accurately in the numerical simulation. It is notable that the diameter of the injected jet is slightly larger than the geometrical diameter used in the engine simulations. As far as the gas-jet width and penetration are concerned, an overall trend can be observed, that is, both become smaller when the nozzle diameter decreases. In the present study, a second order upwind scheme is used to discretize both momentum and continuity equations. Gas injection in KIVA3V was modeled by the Ra et al. [30] procedure

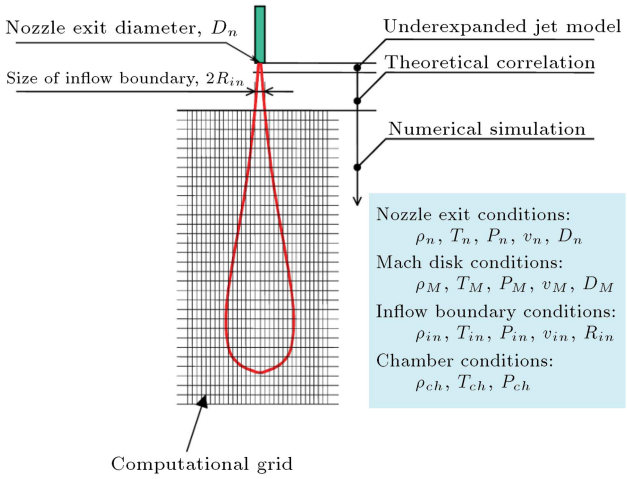

Figure 6. Schematic of the hybrid combination of theoretical and underexpanded jet models [30].

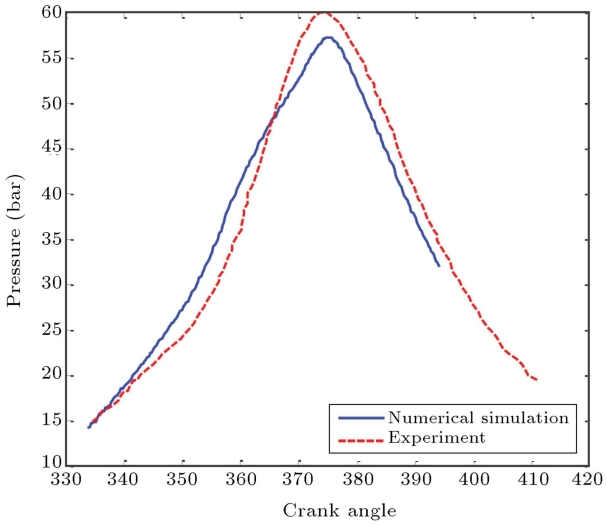

Figure 7. Numerical and experimental in-cylinder pressure of EF7.

which is shown in Figure 6. The present model employed a simplified procedure for under-expanded jet behavior and a theoretical correlation for the turbulent gas jet to obtain the corresponding conditions at the numerical inflow boundaries. As shown in Figure 6, the first part of the jet emerging from the Mach disk is approximated using theoretical gas jet results, and the CFD code only simulates the subsequent gas jet mixing.

3. Results and discussion

In the lack of experimental data for mixture distribution, the in-cylinder pressure of the EF7 engine versus crank angle is compared with numerical simulation and shown in Figure 7. The experiments were performed for the port fuel injection of CNG in the EF7 engine at 1250 rpm and full load operation. Present com-

putations predict in-cylinder pressure with quite good accuracy.

For the evaluation of the mixture, the flammability limits should be defined in terms of mixture Relative Air-Fuel Ratio (RAFR). Based on previous experience with port-injected CNG SI engines [39], in the present work, 0.8 to 1.4 RAFR limits were taken. More specifically, these boundaries should be considered as those defining a stable condition of flame propagation.

The optimization process of an EF7 engine is performed in order to have the best mixture formation to increase the fuel economy of the CNG-DI engine. Our objectives are the percent of flammable mixture near the spark and in the total volume of the cylinder. The spherical volume with a radius of 0.5 mm is selected as the vicinity of spark. A flammable mixture near the spark is essential for the start of ignition. It is also notable that the continuity of the mixture should be kept in order to stable combustion. Operating conditions of direct injection engines over 2500 rpm, whether at high or low loads, are inclined to a homogeneous mixture that is prepared by early fuel injection at the intake process. In this study, we have focused on the stratified stoichiometric mixture already proposed by Bai et al. [40]. This strategy leads to higher CO and lower HC and NOx emissions, which can be effectively after-treated using a three-way catalyst. The stratified stoichiometric mixture can also reduce the knocking phenomena, due to the lean mixture near the walls at the end of combustion. Therefore, we have focused on low engine speeds where this strategy can be implemented. Our operating conditions are confined to the boundaries of the stratified stoichiometric mixture condition. Therefore, 800 rpm (idle) and 2000 rpm are selected.

The results of the optimization process are shown in Figure 8, as points in the plane of objectives according to the flammable mixture close to the spark plug versus total in-cylinder flammability. These optimal designs are found to be able to increase the flammable mixture to improve fuel economy, compared to a baseline engine under the same operating conditions. As shown in this figure, the Pareto front at 2000 rpm is a wide range, while, at 800 rpm, it is narrow. It indicates that objectives at 800 rpm have more connectivity to each other than those of 2000 rpm. Therefore, they can simultaneously improve during optimization.

Some of the designs selected from the Pareto front at 2000 rpm are reported in Table 3. The geometry and injection timing of the Pareto front gave a significant improvement for all cases, with respect to the baseline engine. The results of Table 3 show that goal functions are affected by injection timing, while the geometry is the same for some of the optimum cases. This implies the importance of the start of the injection on goal functions. Moreover, the percent of flammable area near the spark plug has more impact than other goal functions at the start of combustion.

In order to see the sensitivity of the optimization variables to the objective functions, the correlations between the flammable mass of the mixture versus the geometry variable (Ee) are studied for 2000 and 800 rpm, and the results are shown in Figures 9 and 10. Two curves are fitted to the data to understand the effects of the variable on mixture preparation. It is seen from Figure 9(a) that decreasing xEe would increase the flammable mixture near the spark, while it does not have an important effect on total flammability. This trend shows that shallow wide bowl geometry prepares the mixture more appropriately than a deep narrow bowl at 2000 rpm, which leads to enhanced fuel composition. Cubic fitting implies that decreasing cup depth reduces the flammability almost linearly. It is believed that the shallow type bowl geometry utilizes the in-cylinder oxygen more easily, which leads to better mixture distribution. Figure 10 implies that flammability near the spark in the deep narrow bowl is improved, while total in-cylinder flammability does

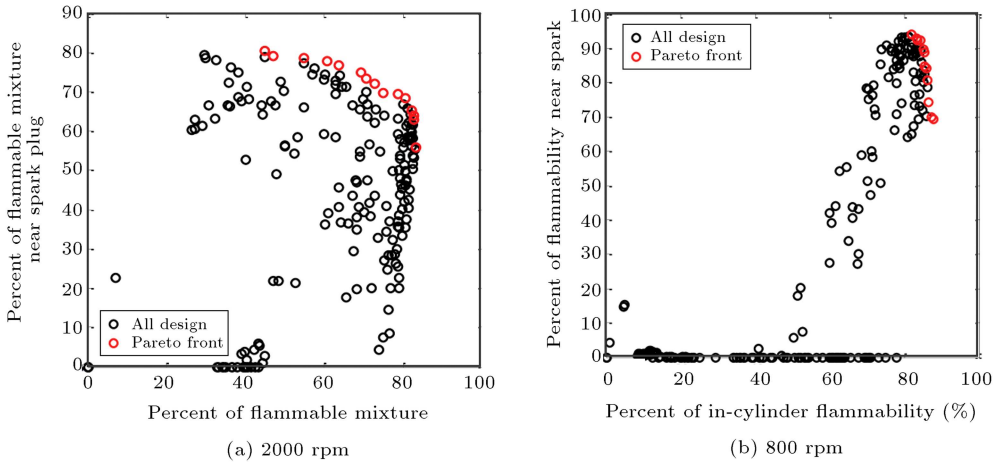

(a) 2000 rpm (b) 800 rpm

Figure 8. Pareto front and results of the optimization process: a) 2000 rpm; and b) 800 rpm.

Table 3. Some of Pareto design at 2000 rpm.

Pareto front	z_{G_p}	z_F	z_E	x_{E_e}	x_E	x_G	x_{G_p}	Start of injection	Percentage of flammable area	Percentage of flammable area near spark plug
Baseline	-29	-24.5	-21.9	-21	-21.5	-18	-17	130CA BTDC	37.5%	0%
1	-26	-21.5	-18.9	-21.9	-22.4	-18.9	-17.9	154CA BTDC	82.5%	62%
2	26	21.5	18.9	21.9	22.4	18.9	17.9	163CA BTDC	67.5%	74%
3	26	21.5	18.9	21.9	22.4	18.9	17.9	155CA BTDC	82.5%	64%
4	26	21.5	18.9	21.9	22.4	18.9	17.9	158CA BTDC	80%	68%
5	26.3	21.8	19.2	21.8	22.3	18.9	17.8	160CA BTDC	74.75%	70%
6	26.3	21.8	19.2	21.8	22.3	18.9	17.8	166CA BTDC	60%	78%
7	26.3	21.8	19.2	21.8	22.3	18.9	17.8	168CA BTDC	55%	78%
8	26	21.5	18.9	21.9	22.4	18.9	17.9	171CA BTDC	45%	80%

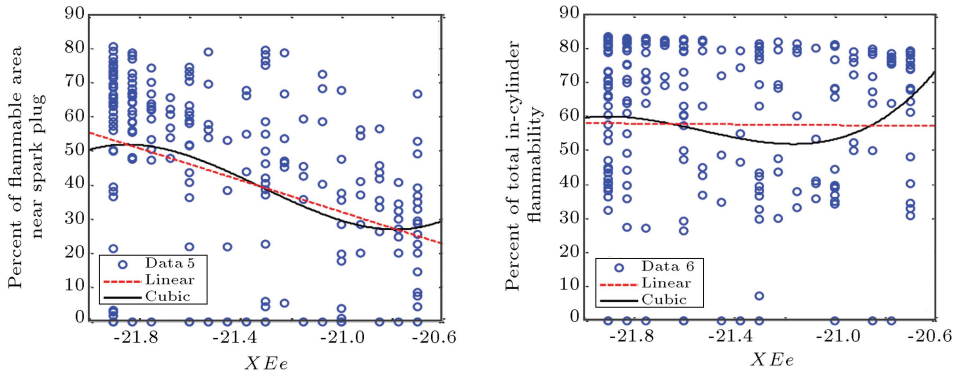

(a) Flammability near spark plug (b) In-cylinder flammability

Figure 9. Effect of combustion bowl geometry on objectives at 2000 rpm: a) Flammability near spark plug; and b) in-cylinder flammability.

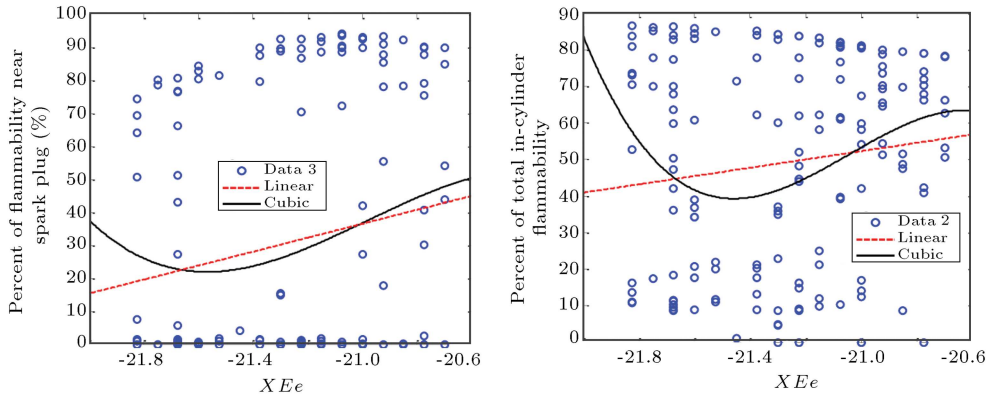

(a) Flammability near spark plug (b) In-cylinder flammability

Figure 10. Effects of combustion bowl geometry on objectives at 800 rpm: a) Flammability near spark plug; and b) in-cylinder flammability.

not significantly vary with variation in geometry at 800 rpm. The linear trend in this figure for total in-cylinder flammability shows a 10 percent improvement, while cubic fitting has a descending trend. Data is scattered in all parts of the plane, as shown in Figure 10, and this distribution does not show a specific trend. This distribution shows that the geometry parameter does not have a distinctive influence on the objectives at 800 rpm.

The effect of piston crown height that corresponds to z_F is shown in Figure 11. This figure verifies that a shallow piston has better mixture distribution than

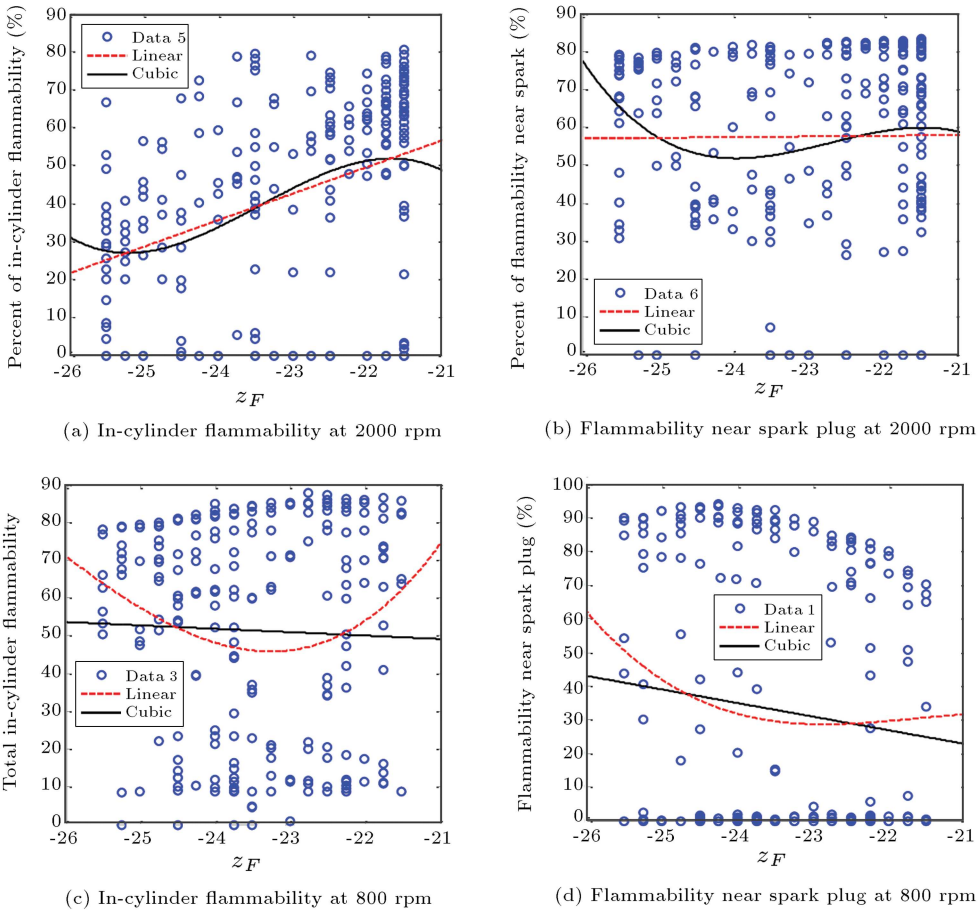

(a) In-cylinder flammability at 2000 rpm

(b) Flammability near spark plug at 2000 rpm

(c) In-cylinder flammability at 800 rpm

(d) Flammability near spark plug at 800 rpm

Figure 11. Effect of combustion bowl geometry on objectives: a) In-cylinder flammability at 2000 rpm; b) flammability near spark plug at 2000 rpm; c) in-cylinder flammability at 800 rpm; and d) flammability near spark plug at 800 rpm.

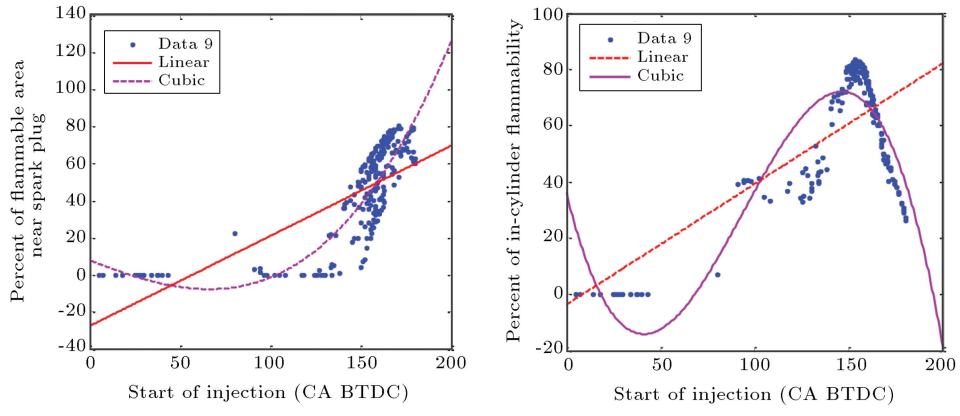

(a) Flammability near spark plug

(b) In-cylinder flammability

Figure 12. Effect of start of injection on objectives at 2000 rpm: a) Flammability near spark plug; and b) in-cylinder flammability.

a deep bowl shape at 2000 rpm. It is notable that geometry does not have an important effect on flammability near the spark plug at 2000 rpm, while it affects at 800 rpm, and decreasing z_F increases flammability near the spark. Total in-cylinder flammability at 800 rpm was not influenced by geometry in the optimum cases, due to early injection of fuel, and is evident from Figure 11(c). When gas is injected too early, there is enough time for mixing, which leads to a nearly homogenous mixture. Therefore, the effect of geometry becomes negligible.

Correlations between mixture formation and injection timing are shown in Figures 12 and 13. In the present study, injection durations of 56° and 23°

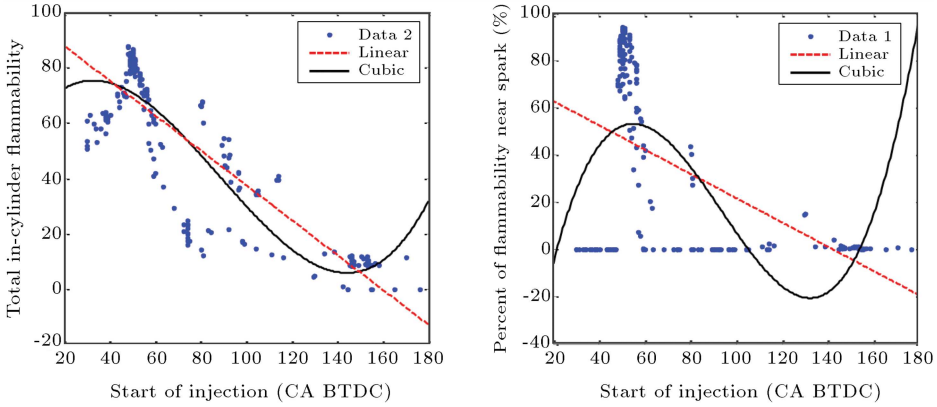

(a) Flammability near spark plug (b) In-cylinder flammability

Figure 13. Effect of start of injection on objectives at 800 rpm: a) Flammability near spark plug; and b) in-cylinder flammability.

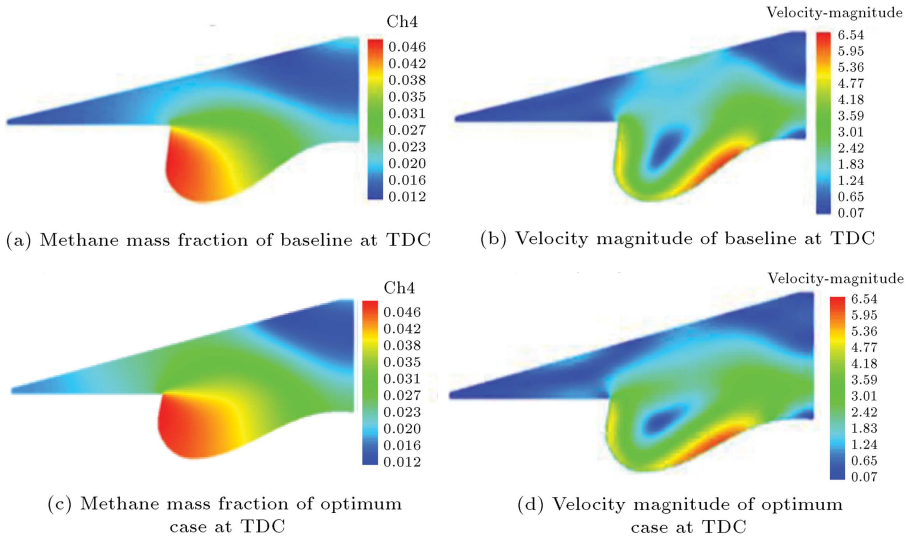

(a) Methane mass fraction of baseline at TDC (b) Velocity magnitude of baseline at TDC

(c) Methane mass fraction of optimum case at TDC (d) Velocity magnitude of optimum case at TDC

Figure 14. Comparison of optimum and baseline cases at 2000 rpm: a) Methane mass fraction of baseline at TDC; b) velocity magnitude of baseline at TDC; c) methane mass fraction of optimum case at TDC; and d) velocity magnitude of optimum case at TDC.

correspond to speeds of 2000 and 800 rpm, respectively. Figure 12(a) and (b) indicate that the optimum injection strategy for the best mixture distribution of the stratified engine is to advance injection timing, while the late injection at 800 rpm would result in better mixture distribution. In the late injection, the gas jet is not influenced by geometry, due to the limited time of diffusion. Therefore, the start of injection has the greatest effect on the results. This justifies the weak independency of the total in-cylinder flammability of Figure 10(b) to geometry constraints. It is also notable that the percent of flammability near the spark is more sensitive to injection timing than total in-cylinder flammability. As shown in this figure, in some finite injection timing, the flammable mass of the mixture is available at the vicinity of the spark, due to the high pressure near the spark plug and special configuration of the piston crown shape. At the appropriate injection timing, natural gas has enough momentum to overcome the pressure of the cylinder head, diffuses to the vicinity of the spark plug, and the flammable mass fraction would be available for the start of stable combustion. Figure 13 also implies that both objectives were simultaneously optimized at specific injection timing. Therefore, both objectives at 800 rpm can be merged into a single function. Figure 13 indicates that there is an optimum for the start of injection at 800 rpm, and it is close to 46 CA BTDC.

Species distribution and the in-cylinder velocity of the optimum case at 2000 rpm were compared to those of the baseline case in Figure 14. As shown in this figure, a significant improvement can be seen in methane distribution, while velocity magnitude is not greatly changed. Methane distribution is more uniform for the optimum case, but a rich mixture was accumulated in the piston crown due to the generated vortex in the combustion chamber. Optimum cases have a shallow type bowl shape and advanced injection

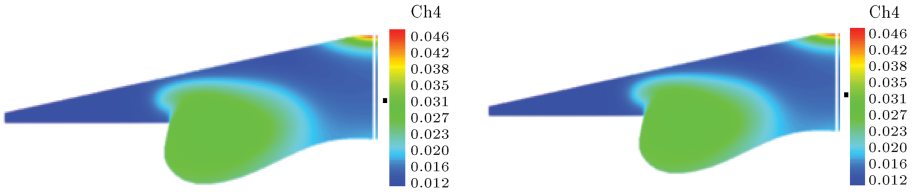

(a) Methane mass fraction of baseline at TDC

(b) Methane mass fraction of optimum case at TDC

Figure 15. Comparison of optimum and baseline cases at 800 rpm: a) Methane mass fraction of baseline at TDC; and b) methane mass fraction of optimum case at TDC.

timing to get the best mixture distribution. Optimum shape decreases the rich mixture and distributes methane in the whole volume of the cylinder head. A narrow bowl piston combustion chamber is not appropriate for charge stratification, because the rich mixture is confined to the piston crown shape, without meeting compactness requirements. Such a combustion chamber is suitable for homogeneous mixture preparation, with advanced SOI. In fact, Figure 14 shows that the resultant fm level at the ignition crank angle increases with larger and more uniform bowl geometry. This could be not true for combustion chambers with flat head pistons, because the recirculation motion of the methane is hindered by the unfavorable chamber section shape onto axial planes.

Figure 15 shows the methane mass fraction of the baseline and one of the Pareto front cases at 800 rpm. As shown in this figure, a considerable improvement of methane distribution near the spark plug can be seen. It is notable that injection timing has a more important effect than geometry on the optimization process. Therefore, the piston crown is not significantly changed during optimization. Flammability near the spark at 800 rpm is a more challenging objective during optimization, because, in many cases, it becomes infinitesimal. Late injection at 800 rpm for a narrow bowl shape piston would result in an aggregation of CNG in the piston crown shape, due to the limited momentum of the injected gas. In a large bore shape and flat head piston, CNG is inclined to the lower pressure part in the combustion chamber, and is accumulated in crevices and low pressure parts. The vicinity of the spark plug at ignition time has the highest pressure of the combustion chamber. Therefore, late injection would not prepare a suitable flammable mixture at the start of combustion near the spark plug. These effects rationalize advanced injection for optimized configuration. It is also notable that a nearly homogeneous mixture is prepared at the start of ignition for 800 rpm, and the connectivity of objectives to each other can be cleared.

4. Conclusions

A multi-dimensional CFD simulations code with a MOGA is introduced for development of a CNG-DI engine. Optimization is focused on piston bowl geometry and injection timing for the development of EF7 to CNG direct injection at low and high speeds. There were seven optimization points related to the combustion chamber geometry and injection timing under different engine operating conditions. The flammable mass of the mixture near the spark plug and total in-cylinder flammability were optimized simultaneously during optimization. The flammable mass near the spark is essential for the start of combustion and total in-cylinder flammability maintains flame propagation. Conclusive remarks are as follows:

- Optimization showed that high-speed operating conditions are more sensitive to combustion chamber geometrical design compared with the low-speed conditions. This is due to the limited time of gas diffusion at high speed in comparison to low speed.
- Total in-cylinder flammability and flammability near the spark at 800 rpm have more connectivity to each other than those of 2000 rpm. Therefore, they can be simultaneously improved during optimization, while the Pareto front at 800 rpm is narrower than 2000 rpm. It is due to a nearly homogenous mixture at 800 rpm.
- At 2000 rpm, the shallow type bowl geometry is more appropriate for the CNG-DI engine because this shape prepares the mixture better than the deep narrow bowl. It is also notable that at low speed, geometry does not have an important effect on mixture distribution.
- The most important effect on mixture distribution at low speed is injection timing, which shows that an almost retarded injection would result in better mixture preparation.
- Among the optimization variables, injection timing is very important and advanced injection for high speed and late injection for low speed would result in optimized fuel economy.

Nomenclature

A	Geometry variable

B	Geometry variable
$Binj$	Geometry variable
BTDC	Before Top Dead Center
BI	Bi-fuel
BSFC	Brake Specific Fuel Consumption
C_p	Heat transfer coefficient ($m^2s^{-2}K^{-1}$)
C_u	Constant
CA	Crank Angle
CO	Carbon monoxide
D	Geometry variable
DI	Direct Injection
D_{kj}	Binary diffusivity for $k-j$ system (m^2t^{-1})
E	Geometry variable
Ee	Geometry variable
EF7	Engine Family 7
F	Geometry variable
G	Geometry variable
Gp	Geometry variable
GDI	Gasoline Direct Injection
h	Enthalpy (kgm^2s^{-2})
Ho	Geometry variable
Hp	Geometry variable
k	Turbulent kinetic energy (m^2s^{-2})
K	Thermal conductivity ($kg.m.s^{-2}.K^{-1}$)
MOGA	Multi Objective Genetic Algorithm
NOx	Nitric oxide
p	pressure ($kgm^{-1}s^{-2}$)
Pr	Prandtl number
R	Term in RNG turbulence model
RNG	Renormalization group
RAFR	Relative Air Fuel Ratio
Sc	Schmidt number
SI	Spark Ignition
T	Temperature (K)
u	Axial velocity (ms^{-1})
x	Longitudinal coordinate
Y	Mass fraction
z	Axial coordinate

Greek symbols

α	Inverse effective Prandtl number
τ	Energy dissipation rate (m^2s^{-3})
μ	Dynamic viscosity ($kg\ m^1s^{-1}$)
ν	Kinematic viscosity (m^2s^{-1})
ρ	Density (kgm^{-3})

Subscripts

eff	Effective
t	Turbulent
T	Theraml

References

1. Baumgarten, C., *Mixture Formation in Internal Combustion Engines*, Springer Berlin, Heidelberg (2006).
2. Croissant, K. and Kendlbacher, C. "Requirements for the engine management system of gasoline direct injection engines", *Direkteinspritzung im Ottomotor Congress*, Essen, Germany (1997).
3. Zhao, F.Q., Lai, M.C., Harrington, D.L. and Engineers, S.O.A., *A Review of Mixture Preparation and Combustion Control Strategies for Spark-Ignited Direct-Injection Gasoline Engines*, Society of Automotive Engineers (1997).
4. Harada, J., Tomita, T., Mizuno, H., Mashiki, Z. and Ito, Y. "Development of direct injection gasoline engine", *SAE Technical Paper 970540*, Detroit, Michigan, United States SAE, pp. (1997).
5. Zeng, K., Huang, Z., Liu, B., Liu, L., Jiang, D., Ren, Y., et al. "Combustion characteristics of a direct-injection natural gas engine under various fuel injection timings", *Applied Thermal Engineering*, **26**, pp. 806-813 (2006).
6. Huang, Z.-H., Liu, L.-X., Jiang, D.-M., Ren, Y., Liu, B., Zeng, K., et al. "Study on cycle-by-cycle variations of combustion in a natural-gas direct-injection engine", *Proceedings of the Institution of Mechanical Engineers, Part D: Journal of Automobile Engineering*, **222**, pp. 1657-1667 (2008).
7. Huang, Z., Shiga, S., Ueda, T., Nakamura, H., Ishima, T., Obokata, T., et al. "Study of cycle-by-cycle variations of natural gas direct injection combustion using a rapid compression machine", *Proceedings of the Institution of Mechanical Engineers, Part D: Journal of Automobile Engineering*, **217**, pp. 53-61 (2003).
8. Huang, Z., Shiga, S., Ueda, T., Nakamura, H., Ishima, T., Obokata, T., et al. "Effect of fuel injection timing relative to ignition timing on the natural-gas direct-injection combustion", *Journal of Engineering for Gas Turbines and Power*, **125**, pp. 783-790 (2003).
9. Huang, Z., Shiga, S., Ueda, T., Jingu, N., Nakamura, H., Ishima, T., et al. "A basic behavior of CNG

DI combustion in a spark-ignited rapid compression machine", *JSME International Journal Series B*, **45**, pp. 891-900 (2002).

10. Shiga, S., Ozone, S., Machacon, H., Karasawa, T., Nakamura, H., Ueda, T., et al. "A study of the combustion and emission characteristics of compressed-natural-gas direct-injection stratified combustion using a rapid-compression-machine", *Combustion and Flame*, **129**, pp. 1-10 (2002).
11. Zheng, J., Wang, J., Wang, B. and Huang, Z. "Effect of the compression ratio on the performance and combustion of a natural-gas direct-injection engine", *Proceedings of the Institution of Mechanical Engineers, Part D: Journal of Automobile Engineering*, **223**, pp. 85-98 (2009).
12. Hassan, M.H., Kalam, M.A., Mahlia, T.I., Aris, I., Nizam, M.K., Abdullah, S., et al. "Experimental test of a new compressed natural gas direct injection engine", *Energy & Fuels*, **23**, pp. 4981-4987 (2009).
13. Kalam, M. and Masjuki, H. "An experimental investigation of high performance natural gas engine with direct injection", *Energy*, **36**, pp. 3563-3571 (2011).
14. Sen, A.K., Zheng, J. and Huang, Z. "Dynamics of cycle-to-cycle variations in a natural gas direct-injection spark-ignition engine", *Applied Energy*, **88**, pp. 2324-2334 (2011).
15. Tadesse, G. and Aziz, A.R.A. "Effect of boost pressure on engine performance and exhaust emissions in direct-injection compressed natural gas (CNG-DI) spark ignition engine", *SAE Paper No 2009-32-0135* (2009).
16. Abdullah, S., Kurniawan, W.H. and Shamsudeen, A. "Numerical analysis of the combustion process in a compressed natural gas direct injection engine", *Journal of Applied Fluid Mechanics*, **1**, pp. 65-86 (2008).
17. Agarwal, A. and Assanis, D. "Multi-dimensional modeling of ignition, combustion and nitric oxide formation in direct injection natural gas engines", *SAE Transactions*, **109**, pp. 1088-1103 (2000).
18. Baratta, M., Catania, A.E., Spessa, E., Herrmann, L. and Roessler, K. "Multi-dimensional modeling of direct natural-gas injection and mixture formation in a stratified-charge si engine with centrally mounted injector", *SAE International Journal of Engines*, **1**, pp. 607-626 (2009).
19. Ali, M.F.M., Kodoguchi, Y., Oka, Y. and Kaida, T. "Improvement of combustion of CNG engine using CNG direct injection and gas-jet ignition method", *SAE Technical Paper 2011-01-1994* (2011).
20. Andreassi, L., Cordiner, S., Mulone, V., Reynolds, C. and Evans, R. "A mixed numerical-experimental analysis for the development of a partially stratified compressed natural gas engine", *ICE 2005 7th International Conference on Engines for Automobile* (2005).
21. Andreassi, L., Facci, A. and Ubertini, S. "Multidimensional modelling of gaseous injection in modern direct injection internal combustion engines: Analisys of different fuel injection strategies", *ICE 2009 9th International Conference on Engines for Automobile* (2009).
22. Douailler, B., Ravet, F., Delpech, V., Soleri, D., Reveille, B. and Kumar, R. "Direct injection of CNG on high compression ratio spark ignition engine: Numerical and experimental investigation", *SAE Technical Paper 2011-01-0923*, Detroit, Michigan, United States (2011).
23. Mohamad, T.I., Yusoff, A., Abdullah, S., Jermy, M., Harrison, M. and Geok, H.H. "The combustion and performance of a converted direct injection compressed natural gas engine using spark plug fuel injector", *SAE Technical Paper 2010-32-0078*, Linz, Austria (2010).
24. Chiodi, M., Berner, H.-J. and Bargene, M. "Investigation on different injection strategies in a direct-injected turbocharged CNG engine", *SAE Technical Paper 2006-01-3000*, Perugia, Italy (2006).
25. Kurniawan, W.H., Abdullah, S., Nopiah, Z.M. and Sopian, K. "The development of artificial neural network for prediction of performance and emissions in a compressed natural gas engine with direct injection system", *SAE Technical Paper 2007-01-4101*, Chicago, Illinois, United States (2007).
26. Kurniawan, W.H., Abdullah, S., Nopiah, Z.M. and Sopian, K. "The application of artificial neural network in predicting and optimizing power and emissions in a compressed natural gas direct injection engine", *SAE Technical Paper 2007-01-4264, 2007*, Rosemont, Illinois, United States (2007).
27. Kurniawan, W.H., Abdullah, S., Nopiah, Z.M. and Sopian, K. "Multi-objective optimization of combustion process in a compressed natural gas direct injection engine using coupled code of CFD and genetic algorithm", *SAE Technical Paper 2007-01-1902* (2007).
28. Amsden, A.A., *Los Alamos National Laboratory Report* (1999).
29. Han, Z. and Reitz, R.D. "Turbulence modeling of internal combustion engines using RNG k-ε models", *Combustion Science and Technology*, **106**, pp. 267-295 (1995).
30. Ra, Y., Kong, S.C., Reitz, R.D., Rutland, C.J. and Han, Z. "Multidimensional modeling of transient gas jet injection using coarse computational grids", *SAE Technical Paper 2005-01-0208*, Detroit, Michigan, United States (2005).
31. Ouellette, P., *Direct Injection of Natural Gas for Diesel Engine Fueling*, Vancouver, B.C., Canada, University of British Columbia (1996).
32. Papageorgakis, G. and Assanis, D.N. "Optimizing gaseous fuel-air mixing in direct injection enginesusing an RNG based k-ε model", *SAE Paper No 980135: SAE* (1998).
33. Kim, G.-H., Kirkpatrick, A. and Mitchell, C. "Computational modeling of natural gas injection in a large

bore engine", *Journal of Engineering for Gas Turbines and Power*, **126**, p. 9 (2004).

34. Park, S.W. "Optimization of combustion chamber geometry for stoichiometric diesel combustion using a micro genetic algorithm", *Fuel Processing Technology*, **91**, pp. 1742-1752 (2010).

35. Genzale, C.L., Reitz, R.D. and Wickman, D.D. "A computational investigation into the effects of spray targeting, bowl geometry and swirl ratio for low-temperature combustion in a heavy-duty diesel engine", *SAE Technical Paper 2007-01-0119*, Detroit, Michigan, United States (2007).

36. Shi, Y. and Reitz, R.D. "Optimization study of the effects of bowl geometry, spray targeting, and swirl ratio for a heavy-duty diesel engine operated at low and high load", *International Journal of Engine Research*, **9**, pp. 325-346 (2008).

37. Kuan, K. and Kou, Y., *Principles of Combustion*, John Wiley & Sons (1986).

38. Chitsaz, I., Saidi, M.H., Mozafari, A.A. and Hajialimohammadi, A. "Experimental and numerical investigation on the jet characteristics of spark ignition direct injection gaseous injector", *Applied Energy*, **105**, p. 8 (2013).

39. Catania, A.E., Misul, D., Spessa, E. and Vassallo, A. "Analysis of combustion parameters and their relation to operating variables and exhaust emissions in an upgraded multivalve bi-fuel CNG SI engine", *SAE Technical Paper 2004-01-0983*, Detroit, Michigan, United States (2004).

40. Bai, Y.-L., Wang, J.-X., Wang, Z. and Shuai, S.-J. "Knocking suppression by stratified stoichiometric mixture with two-zone homogeneity in a DISIengine", *Journal of Engineering for Gas Turbines and Power*, **135**, pp. 012803-012803 (2012).

Biographies

Iman Chitsaz received his PhD degree from Sharif University of Technology (SUT), Tehran, Iran, in 2013. He has been working for six years as an engineer at the Irankhodro Powertrain Co. (IP-CO), and, in 2013, he and his colleges founded a research laboratory there, which investigates injection and combustion phenomena. His research interests include direct injection spark ignition engines, fuel injection systems and optical diagnostic methods for spray and combustion. He is author or co-author of over 15 national and international conference and journal papers.

Mohammad Hassan Saidi is Professor and Chairman of the School of Mechanical Engineering at Sharif University of Technology, Tehran, Iran. His current research interests include MEMS, heat transfer enhancement in boiling and condensation, modeling of pulse tube refrigeration, vortex tube refrigerators, indoor air quality and cleanroom technology, energy efficiency in home appliances, and desiccant cooling systems.

Aliasghar Mozafari received his PhD degree from the University of London (QMC), UK, in 1988. He has been faculty member of the Mechanical Engineering Department at Sharif University of Technology (SUT), Tehran, Iran, for 38 years, Head of the department for six years and Educational Deputy of the department for four years. He has also been member of the Center of Excellence in Energy Conversion, as well as Director of the International Students' Office at SUT. He is author or co-author of over 90 national and international conference and journal papers and has supervised over 40 graduate theses. He has also authored a book, published in 1993.